Two New Black Widow Millisecond Pulsars in M28

Andrew Douglas[1], Prajwal V. Padmanabh[2], Scott M. Ransom[3], Alessandro Ridolfi[2,4], Paulo Freire[2],
Vivek Venkatraman Krishnan[2], Ewan D. Barr[2], Cristina Pallanca[5,6], Mario Cadelano[5,6], Andrea Possenti[4],
Ingrid Stairs[7], Jason W. T. Hessels[8,9], Megan E. DeCesar[10,14], Ryan S. Lynch[11], Matthew Bailes[12], Marta Burgay[4],
David J. Champion[2], Ramesh Karuppusamy[2], Michael Kramer[2], Benjamin Stappers[13], and Laila Vleeschower[13]

[1] University of Virginia, 1826 University Avenue, Charlottesville, VA 22904, USA; adouglas1298@gmail.com
[2] Max-Planck-Institut für Radioastronomie, Auf dem Hügel 69, D-53121 Bonn, Germany
[3] NRAO, 520 Edgemont Road, Charlottesville, VA 22903, USA
[4] INAF—Osservatorio Astronomico di Cagliari, Via della Scienza 5, I-09047 Selargius (CA), Italy
[5] Dipartimento di Fisica e Astronomia "Augusto Righi", Università degli Studi di Bologna, Via Gobetti 93/2, I-40129 Bologna, Italy
[6] INAF-Osservatorio di Astrofisica e Scienze dello Spazio di Bologna, Via Gobetti 93/3, I-40129 Bologna, Italy
[7] Dept. of Physics and Astronomy, University of British Columbia, 6224 Agricultural Road, Vancouver, BC V6T 1Z1, Canada
[8] ASTRON, the Netherlands Institute for Radio Astronomy, Oude Hoogeveensedijk 4, 7991 PD Dwingeloo, The Netherlands
[9] Anton Pannekoek Institute for Astronomy, University of Amsterdam, Postbus 94249, 1090 GE Amsterdam, The Netherlands
[10] George Mason University, Fairfax, VA 22030, USA
[11] Green Bank Observatory, PO Box 2, Green Bank, WV 24944, USA
[12] Centre for Astrophysics and Supercomputing/OzGrav, Swinburne University of Technology, Mail 74, PO Box 218, Hawthorn, Vic, 3122, Australia
[13] Jodrell Bank Centre for Astrophysics, Department of Physics and Astronomy, The University of Manchester, Manchester M13 9PL, UK

Abstract

We report the discovery of two Black Widow millisecond pulsars in the globular cluster (GC) M28 with the MeerKAT telescope. PSR J1824−2452M (M28M) is a 4.78 ms pulsar in a 5.82 hr orbit, and PSR J1824−2452N (M28N) is a 3.35 ms pulsar in a 4.76 hr orbit. Both pulsars have dispersion measures near 119.30 pc cm^{-3} and have low-mass companion stars ($\sim$0.01–0.03 $M_{\odot}$) that do not cause strong radio eclipses or orbital variations. Including these systems, there are now five known black widow pulsars in M28. The pulsar searches were conducted as a part of an initial phase of MeerKAT's GC census (within the TRAPUM Large Survey Project). These faint discoveries demonstrate the advantages of MeerKAT's survey sensitivity over previous searches, and we expect to find additional pulsars in continued searches of this cluster.

Unified Astronomy Thesaurus concepts: Millisecond pulsars (1062); Radio pulsars (1353); Radio astronomy (1338); Globular star clusters (656)

1. Introduction

Globular clusters (GCs) are rich environments for the creation of millisecond pulsars (MSPs; e.g., Ransom 2008). MSPs are created when neutron stars accrete mass and angular momentum from companion stars and are spun up to millisecond periods. Because of the high stellar density in the central regions of GCs between 1000 and 100,000 $M_{\odot}$ pc^{-3},[15] stellar interactions produce dynamically formed binaries that can spin up neutron stars (e.g., Verbunt & Freire 2014). Additionally, these dynamical encounters can produce MSPs in highly eccentric and exotic orbits. Because it is highly likely to find MSPs within GCs, and especially those in exotic orbits, GCs have been the focus of many pulsar searches using the largest radio telescopes. Over 232 GCs have been found so far.[16] Thirty-nine pulsars are currently known in Terzan 5 (hereafter Ter5; Lyne et al. 1990, 2000; Ransom et al. 2005; Hessels et al. 2006; Andersen & Ransom 2018; Cadelano et al. 2018; Ridolfi et al. 2021) and

27 pulsars in 47 Tucanae (hereafter 47Tuc; Manchester et al. 1991; Robinson et al. 1995; Camilo et al. 2000; Pan et al. 2016; Ridolfi et al. 2021). M28 had, up until this work, 12 known pulsars (Bégin 2006), which made it the third cluster in number of known pulsars.[17]

M28 (NGC 6626) is a fairly massive GC in the bulge of the Milky Way at a distance of $\sim$5.4 kpc (Baumgardt & Vasiliev 2021). It contains the first known GC pulsar (PSR B1821−24 or M28A; Lyne et al. 1987), as well as a transitional MSP that behaves alternatively as a radio MSP and as an active X-ray binary (IGR J18245-2452 or M28I; Papitto et al. 2013). M28 has been the subject of many multiwavelength searches in the past few decades. ROSAT observed M28A as a possible X-ray source (Danner et al. 1994), and the Chandra X-ray Observatory has observed the cluster multiple times; in 2011, it confidently located pulsars A, C, D, F, H, J, and K in X-rays (e.g., Bogdanov et al. 2011). The Green Bank Telescope (GBT) also observed M28 multiple times and uncovered 11 radio MSPs in the early to mid-2000s (Bégin 2006). One notable point about these MSPs is that they seem to contain a disproportionately high percentage of Black Widow pulsars, i.e., systems where the companion star is of very low mass ($\leqslant$0.04 $M_{\odot}$), often causing eclipses of the radio pulsations, and having orbits of 2–10 hr in duration (Roberts 2013). M28 also contains two Redback pulsars, i.e.,

---

[14] Resident at the U.S. Naval Research Laboratory, Washington, DC 20375, USA.
[15] Structural Parameters of Globular Clusters: https://people.smp.uq.edu.au/HolgerBaumgardt/globular/parameter.html.
[16] List of pulsars in GCs: http://www.naic.edu/~pfreire/GCpsr.html.

[17] Note that NGC 1851 is now tied with M28: http://www.naic.edu/~pfreire/GCpsr.html.

pulsar binaries with a more massive companion ($\sim$0.1–0.2 $M_\odot$) than the Black Widow systems, but also showing eclipses or timing irregularities, sometime across the entire orbit: Black Widow and Redback pulsars are collectively called spiders (Roberts 2013).

MeerKAT is a newly commissioned 64-dish radio telescope array in South Africa (Booth & Jonas 2012). Two pulsar-based large science projects, MeerTime and TRAPUM, working together as described below, have made observations of several GCs. Initial results from a GC survey targeting clusters with known pulsars for the purposes of comparing older detections with MeerKAT detections has been presented by Ridolfi et al. (2021). With 15 yr since the last dedicated searches (using the GBT), the high sensitivity of MeerKAT coupled with better computing power and the availability of higher-dimension acceleration or "jerk" searches (e.g., Andersen & Ransom 2018) motivated new dedicated searches of M28.

In this paper we present the discovery and timing of M28M and M28N. In Section 2 we present the radio observations and detection of the MSPs and the subsequent timing procedures. In Section 3 we discuss searches for the systems in archival Hubble Space Telescope (HST) and Chandra data. In Section 4 we discuss some implications of these new systems, and in Section 5 we present our conclusions.

2. Observations and Data Analysis

2.1. Data

The initial MeerKAT data that we used to search for new pulsars in M28 were part of the series of survey observations using the core MeerKAT antennas ($\sim$42 out of 64 dishes) that targeted GCs containing known pulsars (Ridolfi et al. 2021). These observations were made as part of a joint effort between the MeerTime project (Bailes et al. 2020), which conducts long-term pulsar timing, and the TRAPUM project (TRansients And PUlsars with MeerKAT; Stappers & Kramer 2016),[18] whose goal is to discover new radio pulsars in targeted regions that have yielded significant discoveries in the past as well as environments that are conducive for pulsar formation.

Two 9000 s duration MeerTime observations occurred on 2019 July 19 and 2020 February 4, with 642 MHz of nominal bandwidth centered at 1283.58 MHz and split into 768 frequency channels. Each channel was coherently dedispersed at a dispersion measure (DM) of 119.892 pc cm^{-3}, which is roughly the average value of the DMs of the known pulsars in the cluster, and was subsequently further frequency subbanded, using incoherent dedispersion, into 256 total-intensity channels with a sampling time of $\sim$76.56 μs. In addition to the two MeerTime observations, we had access to the central beam of two 9000 s TRAPUM observations taken on 2020 December 6 and 11, which were not coherently dedispersed, but had 2048 frequency channels over 856 MHz of bandwidth centered at 1283.86 MHz. These observations used additional antennas to the earlier MeerTime observations, and were therefore approximately 10%–20% more sensitive per unit time than the earlier observations. As with the MeerTime data, these observations were later subbanded after intrachannel dispersion removal into 256 frequency channels and integrated in time to $\sim$76.56 μs samples for analysis. Analysis of the noncentral TRAPUM beams will be published elsewhere.

---

[18] TRAPUM: http://trapum.org.

2.2. Searches

We used PRESTO (Ransom 2011) to perform Fourier domain acceleration and jerk searches on the M28 data using its routine accelsearch (Ransom 2001). The jerk search functionality is a relatively recent addition to PRESTO (Andersen & Ransom 2018). Jerk searching aims to find pulsars whose accelerations are changing linearly during an observation. The jerk term improves search sensitivities to binary pulsars when the integration times (or duration of searched segments) are between 5%–15% of the orbital periods of the pulsars (Bagchi et al. 2013; Andersen & Ransom 2018).

We searched a range of DMs from 115.0 to 125.0 pc cm^{-3}, with a step size of 0.1 pc cm^{-3}. We chose this range as it is roughly centered on the average DM of the pulsars in the cluster, and it would be unlikely that we would find any MSPs significantly outside this range. We conducted differing levels of maximal acceleration and jerk searching (i.e., up to -zmax 200 -wmax 600), where z represents the number of Fourier bins a signal can drift during an observation, and w is the derivative of this. We also conducted acceleration-only searches on shorter segments of the MeerTime data with 29 and 58 million samples, corresponding to around one-third (50 minutes) and two-thirds (100 minutes) of the 117 million sample data file, respectively. This segmented method of searching allows one to detect more compact orbits that would be missed with full-duration acceleration searches. With the TRAPUM data, we conducted segmented searches of 45 and 90 million samples, very roughly one-quarter (60 minutes) and one-half (120 minutes) of the 187 million sample data file, respectively.

We first searched the full-duration observations and segments with acceleration only (-zmax 200), hoping to find a pulsar through the increased sensitivity of MeerKAT, but without success. We then switched to jerk searching, with -zmax 200 and -wmax 600. In the full search, we detected the new M28M at a DM of 119.30 pc cm^{-3} in the 2019 July 19 MeerTime observation at $z = 19.50$ and $w = 10$. We were unable to confirm the pulsar in the 2020 February 4 MeerTime observation (until much later, via folding with an orbital ephemeris) and thus searched the more sensitive TRAPUM observations from 2020 December 6 and 11, and confirmed M28M in these data. We continued searching TRAPUM and MeerTime data at -zmax 200 and -wmax 600, and soon detected a second candidate that we confirmed to be M28N at $z = 3$ and $w = 60$ in the 2020 February 4 data. Because both pulsars were detected in the central TRAPUM beam (0.′246 radius for the December 6 observation and 0.′210 radius for the December 11 observation), we knew the MSPs must be very close to the cluster center.

2.3. Timing

With multiple detections of both new pulsars over the four MeerKAT observations, we were able to determine circular orbits and average barycentric spin periods for each pulsar using the fit_circular_orbit.py routine from PRESTO. These initial ephemerides allowed us to iteratively fold, detect, and determine pulse arrival times from the large number of archival observations of M28 from the GBT, starting in 2005 and continuing to the present day. We note that the spin period of M28M might actually be 9.56 ms, twice the period that we report. The pulsar was initially discovered at that period, but
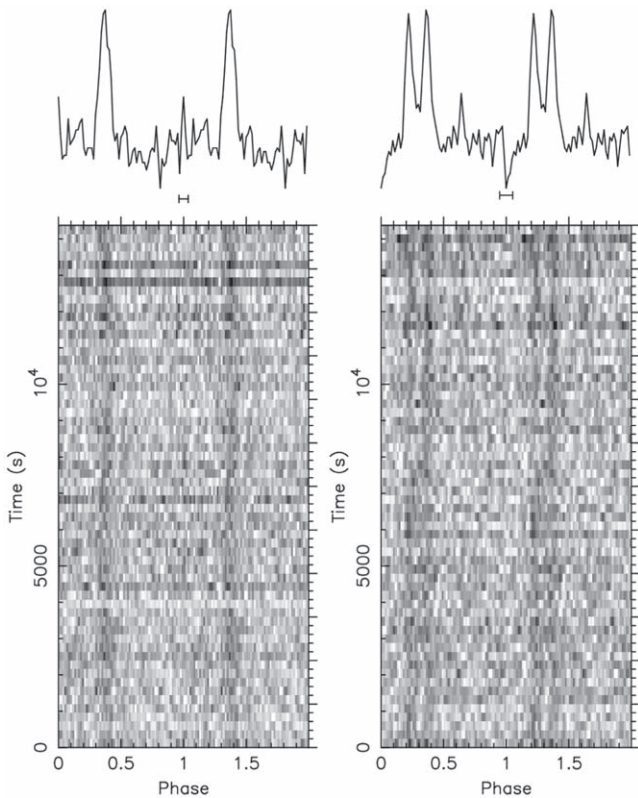
Figure 1. The best detections of M28M and M28N (left and right) from the MeerKAT TRAPUM observation on 2020 December 11. The pulses, each with 64 bins in the profiles, show two full rotations of the pulsar, and the grayscale shows the intensity of the emission as a function of time. The error bar under the summed profiles indicates the approximate time resolution of the data, including dispersive effects, ∼350 μs.

Figure 2. Timing residuals for M28M and M28N. The top two panels show timing residuals as a function of time. The bottom two panels show the timing residuals as a function of orbital phase. Eclipses of the pulsed radio emission would typically occur at superior conjunction, which happens at orbital phase 0.25.

folding of the discovery, subsequent, and archival observations at the longer period show two Gaussian-like peaks with similar amplitudes and widths, and separated by ∼180°. We therefore timed the pulsar assuming it was a 4.78 ms rotator. This ambiguity will be resolved by future MeerTime observations taken with higher time resolution and polarization information.

The GBT data from 2005 to 2008 were a mixture of *L*-band (centered at 1.5 GHz) and *S*-band (centered at 2 GHz) observations initially using the Pulsar Spigot (Kaplan et al. 2005) and having effectively ∼600 MHz of available bandwidth with 1536 frequency channels sampled every 81.92 μs (see Bégin 2006, for more details). Starting in 2010 and continuing through mid-2020, observations were made with the Green Bank Ultimate Pulsar Processing Instrument (GUPPI; DuPlain et al. 2008), using the same bands, but with 512 coherently dedispersed channels, subsequently partially integrated to 128 channels with 40.96 μs sampling. Finally, for the past year, we used VEGAS (Bussa & VEGAS Development Team 2012) in an identical mode to the GUPPI observations.

Both the new pulsars were detected, albeit often with a very low signal-to-noise ratio, in the vast majority of the archival GBT observations. The total GBT integration time, sampled roughly quarterly, is 49.6 hr at *L* band and 73.8 hr at *S* band.

We determined times of arrival (TOAs) for each pulsar using the `get_TOAs.py` routine in `PRESTO` after fitting Gaussians with `PRESTO`'s `pygaussfit.py` to the TRAPUM observation with the highest signal-to-noise ratio (see Figure 1) to use as noiseless pulse templates. We were typically able to obtain roughly one TOA per hour of telescope time with the
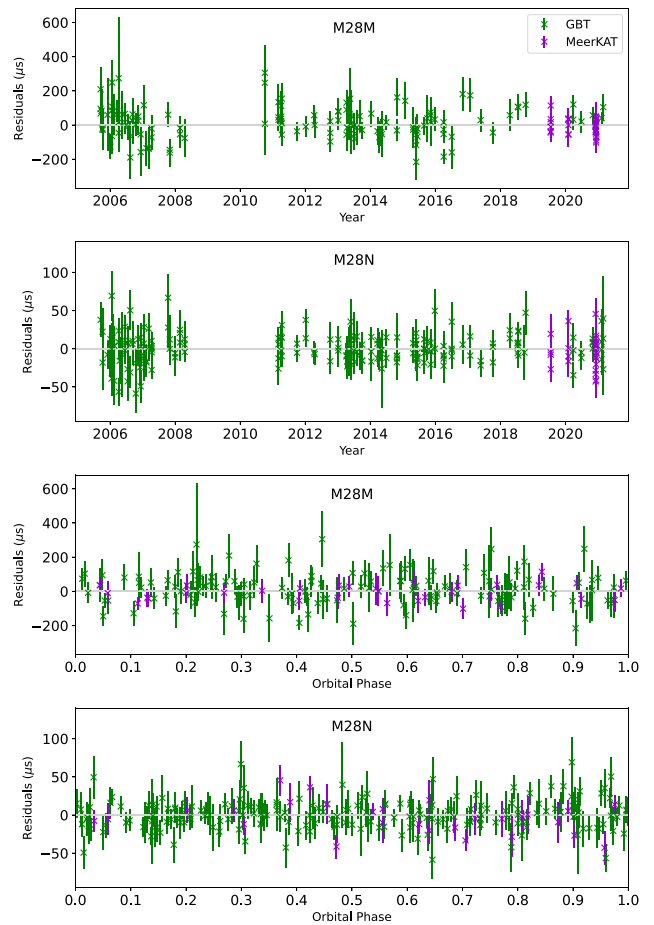
GBT and one per half hour with MeerKAT. These TOAs enabled us to phase connect each pulsar back to 2005 using `TEMPO`,[19] although the slightly fainter M28M required us to use the `DRACULA`[20] software (Freire & Ridolfi 2018) to establish phase connection. The reduced χ^2 values of the fits for both pulsars are near one (1.20 for M28M and 1.01 for M28N), although for M28M, we needed to increase the nominal TOA errors (i.e., using the EFAC parameter) by 50% for Spigot data and 30% for GUPPI/VEGAS/MeerKAT data to achieve that value. The final timing solutions, as well as the plots of the associated timing residuals, are provided in Table 2 and Figure 2.

3. Optical and X-Ray Observations

3.1. Data Set and Data Reduction

To search for the optical counterparts of the two newly discovered binaries M28M and M28N, we use the same archival observations as were used to discover the optical counterparts to M28H and M28I (Pallanca et al. 2010, 2013). The data set is composed of deep and high-resolution optical images acquired with the Wide Field Camera 3 and the
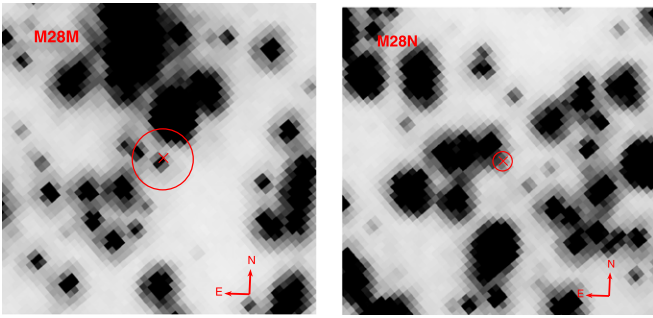

Figure 3. Left-hand panel: $2'' \times 2''$ finding chart of the region around the radio position of M28M. The image is a combination of the F814W images. The red cross is centered on the MSP position, and the red circle has a radius equal to the combined radio and optical positional uncertainties. Right-hand panel: same as in the left-hand panel, but for the case of M28N.

Figure 4. Left-hand panel: CMD of M28 obtained in the F390W−F814W filter combination. Magnitudes have been corrected for the effects of differential reddening following the prescriptions by Cadelano et al. (2020b). The positions of the candidate counterparts to M28M and M28N are highlighted with a red point and a blue square, respectively. Right-hand panel: same as in the left-hand panel, but in the F606W−F814W filter combination.

Advanced Camera for Surveys mounted on the HST. We refer to the aforementioned papers for more details about the adopted data set. The data reduction is performed using DAOPHOT (Stetson 1987) following the prescriptions by Cadelano et al. (2019, 2020a). Instrumental magnitudes are calibrated to the VEGAMAG photometric system using the stars in common with the catalogs presented in Pallanca et al. (2010, 2013). The instrumental positions, after correction for geometric distortions, are transformed in the absolute coordinate systems using the stars in common with the Gaia Early Data Release 3 (Gaia Collaboration et al. 2021). The resulting astrometric uncertainty is about $0''01$. We verify the presence of a possible offset between the radio and optical frames using M28H as reference, whose position is very well measured in both frames. The position of M28H in the Gaia optical frame is R.A. = $18^h24^m31\overset{s}{.}61112$ and decl. = $-24°52'17\overset{''}{.}39856$ and thus differs by about $-0''01$ and $0''18$ in R.A. and decl., respectively, from the radio position quoted in Pallanca et al. (2010). We therefore apply this offset to the optical frame. We cannot include M28I in the offset calculation because its uncertainty in the radio timing position is large.

3.2. Searching for Optical Counterparts

We investigate all of the sources in the area surrounding the positions of the two binaries. In both cases, we find a stellar object in a position that is compatible within the positional uncertainty with that derived from radio data. The finding charts are presented in Figure 3. The candidate optical counterparts to M28M and M28N are displaced from the radio pulsar positions by only ∼$0''05$ and ∼$0''07$, respectively.

In the color–magnitude diagrams (CMDs), the candidate companion to M28M is located along the cluster main sequence, ∼2.9 mag below the turn-off (see Figure 4). Interestingly, it shows a hint of red excess in the F390W(U-band)–F814W(I-band) filter combination, while a small blue excess is detected in the F606W(V-band)–F814W combination. The observations in the H_α narrow filter (i.e., F658N) show no sign of H_α excess.

On the other hand, the candidate companion to M28N is located at ∼5.4 mag below the turn-off and shows a blue excess in all the available filter combinations. Such an excess is commonly observed in exotic binaries such as cataclysmic variables and MSPs (e.g., Rivera Sandoval et al. 2018; Zhao et al. 2019, 2020), and it is usually related to the presence of an accretion disk and/or heating of the secondary star by the
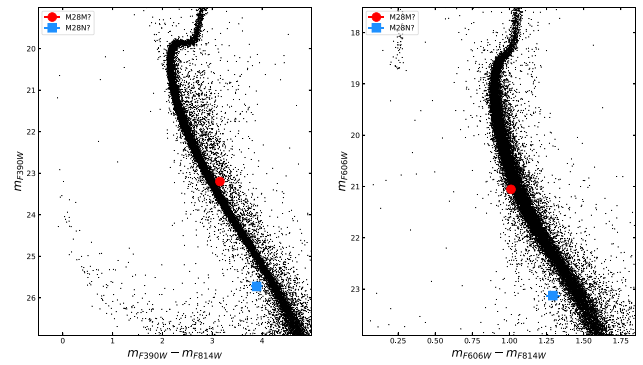
primary. No evidence of H_α excess is detected in this case either.

Despite the good positional agreement and the peculiar CMD positions, the two objects show no sign of photometric variability in any of the available filters. However, companions to Black Widows identified both in GCs and in the Galactic field are often characterized by strong magnitude variations over their short orbital periods. The phenomenon is commonly due to the heating of the companion side exposed to the pulsar wind (e.g., Pallanca et al. 2014; Cadelano et al. 2015; Kaplan et al. 2018; Zharikov et al. 2019). The absence of any magnitude modulation in the proposed candidate companions might suggest that either the two objects are not associated with the pulsars or the heating phenomenon is significantly less efficient than observed in typical Black Widow systems (possibly also due to geometrical effects).

Given all this, we cannot safely conclude that the two proposed counterparts are associated with the MSPs. In fact, the offset positions with respect to the cluster main sequence might also indicate that these two objects are field interlopers rather than cluster members. This possibility might be confirmed in the future through their proper motion analysis. Moreover, the only two Black Widow optical counterparts identified in a GC so far (i.e., PSR J1518+0204C and PSR J1953+1846A; Pallanca et al. 2014; Cadelano et al. 2015) are located 6 to 9 mag below their cluster turn-off (depending on the orbital phase) in the F606W filter. Therefore, the two objects are fainter than the two optical counterparts presented here. This strengthens the likelihood that these two objects are physically not associated with the pulsars, but are unrelated stars belonging either to the M28 population or to the foreground.

3.3. Searching for X-Ray Counterparts

While we did not perform an independent analysis of the multiple Chandra observations of M28, we did query the online Chandra Source Catalog (CSC) v2.0 to see if any point sources matched the positions of the two pulsars. Because the pulsars are only separated by $3''7$, the two closest sources to each pulsar turn out to be the same two CSC sources, 2CXO J182433.0−245210, which was source 29 in Becker et al. (2003) and 2CXO J182433.2−245209, although neither X-ray source is within $1''7$ (more than twice the radius of the formal

X-ray positional errors) of the timing position of either pulsar. The limiting sensitivity of the combined observations at the pulsar positions is $\sim 1.2 \times 10^{-15}$ erg s^{-1}cm^{-2} for M28M and $\sim 1.0 \times 10^{-15}$ erg s^{-1}cm^{-2} for M28N in the ACIS 0.5 -7 keV band, corresponding to luminosity limits of $\lesssim 4.0 \times 10^{30}$ erg s^{-1} and $\lesssim 3.4 \times 10^{30}$ erg s^{-1} for M28M and M28N, respectively, at the 5.37 kpc distance of M28 (Baumgardt & Vasiliev 2021). These limits are similar to the measured ACIS-band luminosities of the many detected millisecond pulsars, including several Black Widows, in the GC 47Tuc (e.g., Bogdanov et al. 2006; Bhattacharya et al. 2017), and are therefore not exceptionally constraining.

4. Discussion

There are many interesting implications from the timing of both M28M and M28N. In this section, we compare the exotic binary population in M28 to that in other GCs, we examine the implications of orbital period derivative measurements (or limits), and we compare the timing-based proper motion measurements with the Gaia-based proper motion of M28 as a whole.

4.1. The Spider Population

A peculiarity of M28 is its fraction of spiders (see Section 1), which is significantly larger than that of 47Tuc and Ter5, the two GCs with the richest content in pulsars to date. In particular, introducing the ratio $\mathcal{R}$ between the population of spiders and the total known pulsar population in a GC, we have $\mathcal{R}_{M28} = 50\%$ (14 known pulsars, which include five Black Widows and two Redbacks; Bégin 2006), $\mathcal{R}_{47Tuc} = 33\%$ (27 known pulsars with six Black Widows and three Redbacks), and $\mathcal{R}_{Ter5} = 13\%$ (two Black Widows and three Redbacks out of a total of 39 known pulsars). Summing over the data for all the other 33 GCs containing known pulsars, the ratio is $\mathcal{R}_{33gc} = 14\%$, close to the value seen in Ter5.[21] However, we focus only on the three aforementioned most populated clusters, as we believe that the sample size for them is large enough that the fraction of spiders can be seen as a trend, at least to first approximation.

Using our knowledge of the numbers of spiders in M28, 47Tuc, and Ter5, we can make a guess as to how many of these types of systems might be potentially observable in the three clusters. Bagchi et al. (2011) used Monte Carlo simulations to predict the number of observable pulsars using six different models. These models predicted M28 to have between 42 and 952 observable pulsars, with an average between the models of 320 ± 60. From the same analysis, Ter5 should have a model averaged pulsar content of 380 ± 40 pulsars and 47Tuc of 160 ± 20 pulsars. It must be noted that there is a large discrepancy in the absolute number of predicted pulsars across the range of these models, but the relative ratios of predicted pulsars in the 3 GCs are roughly compatible between models, with Ter5 predicted to have a total pulsar population 15%–40% larger than M28 and 120%–150% larger than 47Tuc. Combining these percentage intervals with the values of $\mathcal{R}$, we find that M28 should be by far the leading GC in terms of absolute number of spiders, containing about three times the number of spiders than either of the other two GCs, the spider content of which should be similar to each other. In absolute terms, according to the entire range of models explored by

---

Table 1
Comparative Projected Pulsar Populations in M28, 47Tuc, and Ter5

Cluster Properties	M28	47 Tucanae	Terzan 5
Average Potential Observable MSPs	320 ± 60	160 ± 20	380 ± 40
Ratio of Spider Systems to Known MSPs ($\mathcal{R}$)	0.50	0.33	0.13
Mass Density within the Half-mass Radius ($\log \rho_{hm}$)	3.49	2.65	3.34

Note. These are the relevant values taken from Section 4.1.

Bagchi et al. (2011), M28 might host from ~ 20 observable spiders up to ~ 400, while assuming a conservative log-normal distribution in the pulsar luminosity, the simulations of Bagchi et al. (2011) indicate a number of potentially observable spiders in M28 ranging from ~ 20 to ~ 80.

These results naturally raise the question about the reasons for the overabundance of spiders in M28 with respect to other GCs, and in particular, 47Tuc and Ter5. It is well known that the formation of spiders in a GC can occur via two channels: ordinary binary evolution (as in the Galactic field), or through the occurrence of three- or four-body dynamical interactions, which can support the creation of new binaries with suitable parameters to later become spiders. The former pathway certainly depends on the total mass M_{GC} of the GC, while the latter process is in turn favored by a crowded and massive stellar environment, suggesting an exploration of both the role of the rate Γ_c of stellar interactions in the core (which depends on the central density, ρ_c, and the core radius of the GC, r_c, $\Gamma_c = \rho_c^{3/2} r_c^2$; see e.g., Verbunt & Freire 2014), and of the mass density within the half-mass radius ρ_{hm}. Using the data provided in the website by Holger and Baumgardt,[22] as far as the values of the total mass, Ter5, 47Tuc, and M28 (sorted in this way) appear in the top 23% of the listed GCs. They are also in the top 22% in terms of interaction rate in the core (with Ter5 leading M28 and 47Tuc). As for ρ_{hm}, M28 (sixth position) and Ter5 (ninth position) fell in the top 10% of the GCs, with 47Tuc in the top 27%. The high ranking in all the mentioned lists is in agreement with the observed occurrence of a high number of millisecond pulsars in the three clusters. However, M28 prevails among the three clusters only in terms of mass density within the half-mass radius, with a limited edge on Ter5, i.e., $\log \rho_{hm,M28} = 3.49$, and $\log \rho_{hm,Ter5} = 3.34$. On the other hand, despite a similar predicted number of spiders (see above), Ter5 and 47Tuc show significantly different values of the latter parameter ($\log \rho_{hm,47Tuc} = 2.65$), as well as of Γ_c (three times larger in Ter5 than in 47Tuc), having only similar values for the total mass. These values are summarized in Table 1.

In summary, in addition to the suggested impact of ρ_{hm}, which could be explored with detailed simulations of its effects on the production of the spiders, some other still unassessed and/or as yet unmeasured parameters are at play in determining the population of spiders in a cluster, e.g., one can think about the fraction of binaries, or the past dynamical history of the cluster. An interesting indication could arise from the distinct rarity of eclipses in the sample of the M28 spiders. In fact, of the five Black Widow systems, only one shows obvious eclipses, M28G (Bégin 2006). The timing analyses of these

---

[21] All the numbers are taken from https://www.naic.edu/~pfreire/GCpsr.html.

[22] Structural Parameters of Globular Clusters: https://people.smp.uq.edu.au/HolgerBaumgardt/globular/parameter.html.

systems do not display strong orbital variability either, which is very commonly detected in similar systems. In principle, these peculiarities could be due to a geometrical effect, i.e., we are looking at the systems nearly face on, or at an inclination of near 0°. However, this is statistically unlikely to occur for many binary systems at once. An alternative option is that the relative absence of eclipses and the orbital stability are indications that the companion star is stable and there is little stellar wind being ablated. This often implies that the systems have had time to stabilize and hence are older than the typical population of spiders in GCs. If this hypothesis is supported by additional observations and further discoveries in M28, it would suggest that the high number of spiders in this GC is sustained by an accumulation mechanism, where the spiders were produced far in the past, but have managed to survive intact in the cluster environment.

4.2. Corrections for Pulse Period Derivative

Pulsars in GCs are often found to have seemingly nonphysical values of $\dot{P}$ compared to pulsars in the Galaxy. This contamination is primarily a result of the acceleration of the pulsar in the gravitational field of the cluster and leaves no vestige of the intrinsic period derivative in the observed period derivative (Phinney 1992). In order to solve for the intrinsic period derivative $\dot{P}_{\mathrm{int}}$, we can (e.g., Freire et al. 2017) use the equation

$$\frac{\dot{P}_{\mathrm{obs}}}{P} = \frac{\dot{P}_{\mathrm{int}}}{P} + \frac{\mu^2 d}{c} + \frac{a_{l,\mathrm{GC}}}{c} + \frac{a_{l,\mathrm{gal}}}{c}, \qquad (1)$$

where $\dot{P}_{\mathrm{obs}}$ is the observed spin-period derivative. The second term on the right represents the Shklovskii effect (Shklovskii 1970) due to the motion of the pulsar in the plane of the sky, μ is the proper motion of the cluster, d is the distance to the cluster, and c is the speed of light. The third term, $a_{l,\mathrm{GC}}$ represents the line-of-sight acceleration of the pulsar in the GC. The fourth term represents the difference in acceleration, $a_{l,\mathrm{gal}}$, between the solar system and the cluster in the field of the galaxy.

The Shklovskii effect may be calculated as 3.12×10^{-10} m s^{-2} using the total proper motion of the cluster (8.9 mas yr^{-1}) and its 5.37 kpc distance (Vasiliev & Baumgardt 2021; Baumgardt & Vasiliev 2021). The Galactic acceleration may be computed as 3.08×10^{-10} m s^{-2} using the Galactic coordinates of M28 and its distance (e.g., Freire et al. 2017). The line-of-sight acceleration from the cluster may then be solved for using

$$a_{l,\mathrm{GC}} = \frac{\dot{P}_{b,\mathrm{obs}}}{P_b} c - \mu^2 d - a_{l,\mathrm{gal}}, \qquad (2)$$

where P_b and $\dot{P}_{b,\mathrm{obs}}$ are the orbital period and its observed period derivative. For M28N, which has a more significant measurement of $\dot{P}_{b,\mathrm{obs}}$, the cluster acceleration is 1.02×10^{-8} m s^{-2}. With this value, we can then solve for $\dot{P}_{\mathrm{int}}$ with Equation (1), giving $\sim 3.8 \times 10^{-20}$ for M28N, and allowing estimates of the spin-down based physical parameters in Table 2.

With a less precise measurement of $\dot{P}_{b,\mathrm{obs}}$ for M28M, we can assume a 95% lower limit of the true $\dot{P}_{b,\mathrm{obs}}$ of 4.4×10^{-13} given the estimated error on $\dot{P}_{b,\mathrm{obs}}$ and then proceed in a similar manner for M28N to obtain an upper limit of $\dot{P}_{\mathrm{int}} < 2.2 \times 10^{-20}$ with corresponding upper limits (magnetic field and $\dot{E}$) or lower limits

Table 2
New MeerKAT Discovered M28 Pulsars

Parameter	Value(Error)	Value(Error)
Pulsar Name	J1824−2452M	J1824−2452N
R.A. (J2000)	$18^h\,24^m\,33\overset{s}{.}1835(5)$	$18^h\,24^m\,33\overset{s}{.}1418(12)$
Decl. (J2000)	$-24°\,52'\,08\overset{''}{.}2(23)$	$-24°\,52'\,11\overset{''}{.}89(3)$
Proper Motion R.A. (mas yr^{-1})	0.0(1.4)	0.5(0.3)
Proper Motion decl. (mas yr^{-1})	$-23(28)$	$-15(6)$
Pulsar Period (ms)	4.7842842982785(7)	3.35287243686099(10)
Pulsar Frequency (Hz)	209.01767906222(3)	298.251728579395(9)
Frequency Derivative (Hz s^{-1})	$-5.36572(12) \times 10^{-15}$	$-1.416227(3) \times 10^{-14}$
Frequency Second Derivative (Hz s^{-2})	$-1.4(4) \times 10^{-26}$	$-9.4(1.2) \times 10^{-27}$
Reference Epoch (MJD)	56,450	56,450
Dispersion Measure (pc cm^{-3})	119.352(11)	119.321(3)
Orbital Period (days)	0.2425192190(14)	0.19849331510(11)
Orbital Period Derivative	$3.1(1.6) \times 10^{-12}$	$6.2(1.4) \times 10^{-13}$
Projected Semimajor Axis (lt-s)	0.032463(8)	0.0497303(16)
Time of Ascending Node	56,451.272704(15)	56,451.2896713(15)
Properties of Fit		
Span of Timing Data (MJD)	53,629–59,274	53,629–59,274
Number of TOAs	161	230
rms TOA Residual (μs)	71.11	16.45
Derived Parameters		
Mass Function ($M_\odot$)	$6.245(4) \times 10^{-7}$	$3.3516(3) \times 10^{-6}$
Min Companion Mass ($M_\odot$)	$\geqslant 0.011$	$\geqslant 0.019$
Pulsar Magnetic Field (G)[a]	$< 4 \times 10^8$	3.6×10^8
Pulsar Age (yr)[a]	$> 3 \times 10^9$	1.4×10^9
Pulsar $\dot{E}$ (erg s^{-1})[a]	$< 8 \times 10^{33}$	4.0×10^{34}
Flux Density at 2 GHz (μJy)	6(3)	10(5)
Angular Offset of Cluster Center (mas)	5.092	3.464
Total Proper Motion[b] (mas yr^{-1})	10(22)	14(7)

Notes. Numbers in parentheses represent 1σ uncertainties in the last digit. The timing solution was determined using TEMPO with the DE440 (Park et al. 2021) solar system ephemeris and the ELL1 binary model. The time system used is barycentric dynamical time (TDB), referenced to TT via BIPM. The minimum companion mass was calculated assuming a pulsar mass of 1.4 $M_\odot$.
[a] Here we assumed a 95% lower limit to $\dot{P}_b$, which allowed us to solve for an upper limit on the intrinsic $\dot{P}$ and therefore a lower limit on the age and upper limits on the magnetic field and $\dot{E}$ (see Section 4.2).
[b] The relatively poorly constrained proper motions are nevertheless consistent with the overall cluster proper motion measured by Gaia (see Section 4.3).

(characteristic age) on the resulting physical spin-down parameters in Table 2 (denoted by †).

4.3. Proper Motions

The long timing baseline provided by the GBT data allows low-precision estimates of the individual pulsar proper motions

as well as of the orbital period derivatives mentioned in the previous section. The Gaia mission has measured the proper motion of M28 as $\mu_\alpha = -0.28(3)$ mas yr^{-1} and $\mu_\delta = -8.92(3)$ mas yr^{-1} for a total proper motion of 8.92(3) mas yr^{-1} (Vasiliev & Baumgardt 2021). The timing-based proper motions (or limits on measurements) are consistent with the Gaia values within one sigma. This supports the scenario that the two binary systems are associated with M28 and are bound to the cluster.

5. Summary and Ramifications

We used sensitive new TRAPUM and MeerTime data to detect two new Black Widow pulsars in the GC M28 and exploited archival GBT observations of the cluster to determine long-term coherent timing solutions for the two binary pulsars. Their orbital parameters reflect the typical values seen in Black Widow systems in other GCs. However, their discovery supports the growing evidence that the structural parameters and the internal dynamics of M28 make it a very effective factory of exotic pulsar binaries, here defined as the joint class of Black Widow and Redback systems. Half of the known pulsars in M28 belong to these categories, and projecting this high fraction on preceding pulsar population studies, M28 could harbor several tens or even some hundreds of these binaries. Some of them could be unveiled during the ongoing search of the outer beams of the TRAPUM observations. We also searched for the companions (or overall systems) of M28M and M28N in the optical and X-ray bands, but were unable to conclusively identify either system in either band.

In addition to confirming the sensitivity and the potential of the MeerKAT telescope to find new pulsars in GCs (with these discoveries, the total count for MeerKAT reaches 36 new pulsars[23]), the case of M28M and M28N also highlights the value of the long-term monitoring and archiving of GC pulsar data. As in the case of Ter5 (Ridolfi et al. 2021), the use of archival GBT data allowed us to establish for M28M and M28N a ~16 yr long timing solution soon after the discovery of these pulsars. This is especially important for the data from large single-dish telescopes, such as the GBT, which have wider beams and very likely include the positions of newly discovered pulsars.

In this context, it is worth noting that M28M and M28N were not discovered in the GBT data because they are, on most occasions, too faint to be detected by blind-search algorithms. However, after their orbits had been characterized in the MeerKAT observations, the number of trials necessary for a detection decreased dramatically. This implied that the pulsed signals from these objects could be recovered in the archival GBT data with a signal-to-noise ratio high enough for determining a suitable set of pulse times of arrival and then deriving a phase-connected timing solution with highly precise timing parameters. For these reasons, it is clear that the current archival data of many GCs will continue to be of great use for a fast characterization of many MeerKAT discoveries. The same also applies, of course, for the archival data from HST and from high-energy telescopes, which are also important to immediately investigate the new pulsars at these wavelengths.

The MeerKAT telescope is operated by the South African Radio Astronomy Observatory, which is a facility of the

ORCID iDs

Andrew Douglas ⓘ https://orcid.org/0000-0001-5492-4215
Prajwal V. Padmanabh ⓘ https://orcid.org/0000-0001-5624-4635
Scott M. Ransom ⓘ https://orcid.org/0000-0001-5799-9714
Alessandro Ridolfi ⓘ https://orcid.org/0000-0001-6762-2638
Paulo Freire ⓘ https://orcid.org/0000-0003-1307-9435
Vivek Venkatraman Krishnan ⓘ https://orcid.org/0000-0001-9518-9819
Ewan D. Barr ⓘ https://orcid.org/0000-0001-8715-9628
Cristina Pallanca ⓘ https://orcid.org/0000-0002-7104-2107
Mario Cadelano ⓘ https://orcid.org/0000-0002-5038-3914
Andrea Possenti ⓘ https://orcid.org/0000-0001-5902-3731
Ingrid Stairs ⓘ https://orcid.org/0000-0001-9784-8670
Jason W. T. Hessels ⓘ https://orcid.org/0000-0003-2317-1446
Megan E. DeCesar ⓘ https://orcid.org/0000-0002-2185-1790
Ryan S. Lynch ⓘ https://orcid.org/0000-0001-5229-7430
Matthew Bailes ⓘ https://orcid.org/0000-0003-3294-3081
Marta Burgay ⓘ https://orcid.org/0000-0002-8265-4344
David J. Champion ⓘ https://orcid.org/0000-0003-1361-7723
Ramesh Karuppusamy ⓘ https://orcid.org/0000-0002-5307-2919

---

[23] http://trapum.org/discoveries.html

Michael Kramer ⊙ https://orcid.org/0000-0002-4175-2271
Benjamin Stappers ⊙ https://orcid.org/0000-0001-9242-7041
Laila Vleeschower ⊙ https://orcid.org/0000-0003-0292-4453

References

Andersen, B. C., & Ransom, S. M. 2018, ApJL, 863, L13
Astropy Collaboration, Robitaille, T. P., Tollerud, E. J., et al. 2013, A&A, 558, A33
Bagchi, M., Lorimer, D. R., & Chennamangalam, J. 2011, MNRAS, 418, 477
Bagchi, M., Lorimer, D. R., & Wolfe, S. 2013, MNRAS, 432, 1303
Bailes, M., Jameson, A., Abbate, F., et al. 2020, PASA, 37, e028
Baumgardt, H., & Vasiliev, E. 2021, MNRAS, 505, 5957
Becker, W., Swartz, D. A., Pavlov, G. G., et al. 2003, ApJ, 594, 798
Bégin, S. 2006, Master's thesis, Univ. of British Columbia, doi:10.14288/1.0085181
Bhattacharya, S., Heinke, C. O., Chugunov, A. I., et al. 2017, MNRAS, 472, 3706
Bogdanov, S., Grindlay, J. E., Heinke, C. O., et al. 2006, ApJ, 646, 1104
Bogdanov, S., van den Berg, M., Servillat, M., et al. 2011, ApJ, 730, 81
Booth, R. S., & Jonas, J. L. 2012, AfrSk, 16, 101
Bussa, S. & VEGAS Development Team 2012, AAS Meeting, 219, 446.10
Cadelano, M., Chen, J., Pallanca, C., et al. 2020a, ApJ, 905, 63
Cadelano, M., Ferraro, F. R., Istrate, A. G., et al. 2019, ApJ, 875, 25
Cadelano, M., Pallanca, C., Ferraro, F. R., et al. 2015, ApJ, 807, 91
Cadelano, M., Ransom, S. M., Freire, P. C. C., et al. 2018, ApJ, 855, 125
Cadelano, M., Saracino, S., Dalessandro, E., et al. 2020b, ApJ, 895, 54
Camilo, F., Lorimer, D. R., Freire, P., Lyne, A. G., & Manchester, R. N. 2000, ApJ, 535, 975
Danner, R., Kulkarni, S. R., & Thorsett, S. E. 1994, ApJL, 436, L153
DuPlain, R., Ransom, S., Demorest, P., et al. 2008, Proc. SPIE, 7019, 70191D
Freire, P. C. C., & Ridolfi, A. 2018, MNRAS, 476, 4794
Freire, P. C. C., Ridolfi, A., Kramer, M., et al. 2017, MNRAS, 471, 857
Gaia Collaboration, Brown, A. G. A., Vallenari, A., et al. 2021, A&A, 649, A1
Hessels, J. W. T., Ransom, S. M., Stairs, I. H., et al. 2006, Sci, 311, 1901
Kaplan, D., Escoffier, R., Lacasse, R., et al. 2005, PASP, 117, 643
Kaplan, D. L., Stovall, K., van Kerkwijk, M. H., Fremling, C., & Istrate, A. G. 2018, ApJ, 864, 15
Lyne, A. G., Brinklow, A., Middleditch, J., Kulkarni, S. R., & Backer, D. C. 1987, Natur, 328, 399
Lyne, A. G., Manchester, R. N., D'Amico, N., et al. 1990, Natur, 347, 650
Lyne, A. G., Mankelow, S. H., Bell, J. F., & Manchester, R. N. 2000, MNRAS, 316, 491
Manchester, R. N., Lyne, A. G., Robinson, C., et al. 1991, Natur, 352, 219
Pallanca, C., Dalessandro, E., Ferraro, F. R., et al. 2010, ApJ, 725, 1165
Pallanca, C., Dalessandro, E., Ferraro, F. R., Lanzoni, B., & Beccari, G. 2013, ApJ, 773, 122
Pallanca, C., Ransom, S. M., Ferraro, F. R., et al. 2014, ApJ, 795, 29
Pan, Z., Hobbs, G., Li, D., et al. 2016, MNRAS, 459, L26
Papitto, A., Ferrigno, C., Bozzo, E., et al. 2013, Natur, 501, 517
Park, R. S., Folkner, W. M., Williams, J. G., & Boggs, D. H. 2021, AJ, 161, 105
Phinney, E. S. 1992, RSPTA, 341, 39
Ransom, S. 2011, PRESTO: PulsaR Exploration and Search TOolkit, Astrophysics Source Code Library, ascl:1107.017
Ransom, S. M. 2001, PhD thesis, Harvard Univ.
Ransom, S. M. 2008, in IAU Symp. 246, Dynamical Evolution of Dense Stellar Systems, ed. E. Vesperini, M. Giersz, & A. Sills (Cambridge: Cambridge Univ. Press), 291
Ransom, S. M., Hessels, J. W. T., Stairs, I. H., et al. 2005, Sci, 307, 892
Ridolfi, A., Gautam, T., Freire, P. C. C., et al. 2021, MNRAS, 504, 1407
Rivera Sandoval, L. E., van den Berg, M., Heinke, C. O., et al. 2018, MNRAS, 475, 4841
Roberts, M. S. E. 2013, in IAU Symp. 291, Neutron Stars and Pulsars: Challenges and Opportunities after 80 Years, ed. J. van Leeuwen (Cambridge: Cambridge Univ. Press), 127
Robinson, C., Lyne, A. G., Manchester, R. N., et al. 1995, MNRAS, 274, 547
Shklovskii, I. S. 1970, SvA, 13, 562
Stappers, B., & Kramer, M. 2016, in Proc. Science 277, MeerKAT Science: On the Pathway to the SKA (Trieste: Sissa), 9
Stetson, P. B. 1987, PASP, 99, 191
van Straten, W., Demorest, P., Khoo, J., et al. 2011, PSRCHIVE: Development Library for the Analysis of Pulsar Astronomical Data, Astrophysics Source Code Library, ascl:1105.014
Vasiliev, E., & Baumgardt, H. 2021, MNRAS, 505, 5978
Verbunt, F., & Freire, P. C. C. 2014, A&A, 561, A11
Zhao, Y., Heinke, C. O., Cohn, H. N., et al. 2020, MNRAS, 499, 3338
Zhao, Y., Heinke, C. O., Cohn, H. N., Lugger, P. M., & Cool, A. M. 2019, MNRAS, 483, 4560
Zharikov, S., Kirichenko, A., Zyuzin, D., Shibanov, Y., & Deneva, J. S. 2019, MNRAS, 489, 5547